ACS APPLIED MATERIALS & INTERFACES

www.acsami.org

Research Article

# Efficient and Stable Blue Perovskite Light-Emitting Devices Based on Inorganic $Cs_4PbBr_6$ Spaced Low-Dimensional $CsPbBr_3$ through Synergistic Control of Amino Alcohols and Polymer Additives

Li Song,* Lixin Huang, Yuan Liu, Yongsheng Hu,* Xiaoyang Guo,* Yulei Chang, Chong Geng, Shu Xu, Zihui Zhang, Yonghui Zhang, and Nannan Luan

Cite This: *ACS Appl. Mater. Interfaces* 2021, 13, 33199–33208

Read Online

ACCESS | Metrics & More | Article Recommendations | Supporting Information

**ABSTRACT:** Perovskite light-emitting devices (PeLEDs) have drawn a great deal of attention because of their exceptional optical and electrical properties. However, as for the blue PeLEDs based on low-dimensional (LD) $CsPbBr_3$, the low conductivity of the widely used organic spacers as well as the difficulty of forming pure and uniform LD $CsPbBr_3$ phase have severely inhibited the device performance such as stability and efficiency. In this work, we report an effective strategy to obtain high-quality LD $CsPbBr_3$ by using a novel spacer of inorganic $Cs_4PbBr_6$ instead of the common long-chain ammonium halides. We found that a 3-amino-1-propanol (3AP)-modified PEDOT:PSS was helpful to stimulate the formation of the LD blue emissive $CsPbBr_3$:$Cs_4PbBr_6$ composite. We also revealed that an additive of poly(vinylpyrrolidone) (PVP) in the precursor can limit further growth of LD perovskite phase into 3D perovskite phase upon annealing, thus resulting in a uniformly distributed LD perovskite with high color stability. Consequently, efficient blue PeLEDs @ 485 nm with a brightness of 2192 cd/m$^2$, current efficiency of 2.68 cd/A, and external quantum efficiency of 2.3% was successfully achieved. More importantly, the device showed much improved working stability compared to those with the spacer of organic ammonium halides. Our results provide some helpful insights into developing efficient and stable blue PeLEDs.

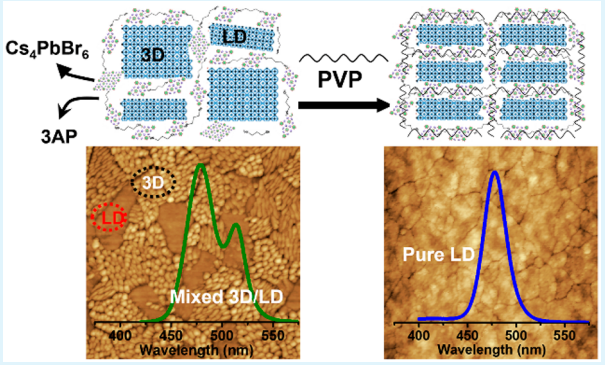


**KEYWORDS:** *all-inorganic perovskite, inorganic spacer, light-emitting, $Cs_4PbBr_6$, polymer scaffold*



## INTRODUCTION

Metal halide perovskites have shown great potential in the fields of optoelectronic devices becauses of their exceptional optical and electrical properties such as high carrier mobility, high photoluminescence quantum efficiency (PLQE), flexibly tunable band gaps, and high color purity.[1−3] So far, perovskite light-emitting devices (PeLEDs) with external quantum efficiency (EQE) exceeding 20% have been achieved in the near-infrared and green emissions.[1,4−10] However, because of the lack of a stable and efficient blue perovskite emission layer, the performance for blue PeLEDs, which is indispensable for practical applications, still remains challenging.[11,12]

Composition engineering by incorporating chlorine into bromine-based perovskite is one commonly adopted strategy to achieve blue emission. However, the unavoidable ion migration and phase segregation make the mixed-halide blue PeLEDs suffer from unstable EL emission and spectra shift, which is detrimental in display applications.[13−15] Another widely adopted approach for blue emission is to construct quasi-two-dimensional (2D) perovskite by virtue of the quantum confinement effect.[11,16,17] Generally, long-chain organic ligands[16,18−23] such as phenylethylammonium (PEA), butylammonium (BA), and ethylammonium (EA) are introduced as spacers to tailor the thickness of the perovskite layers and tune their optoelectronic properties. Generally, the more organic spacers, the greater the blue shift for the spectra. However, the insulation characteristic of the organic spacers will decrease the carrier conductivity of the perovskite film significantly, limiting the brightness of the devices. Moreover, the poor conductivity may also cause a large amount of Joule heat, which is one of the key factors limiting the device stability.[24,25] Therefore, it is highly desirable to develop novel spacers, especially with a pure bromide (rather than mixed halide) system, to improve the device performance.

Received: February 6, 2021
Accepted: June 21, 2021
Published: July 7, 2021

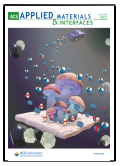




https://doi.org/10.1021/acsami.1c02555
*ACS Appl. Mater. Interfaces* 2021, 13, 33199−33208

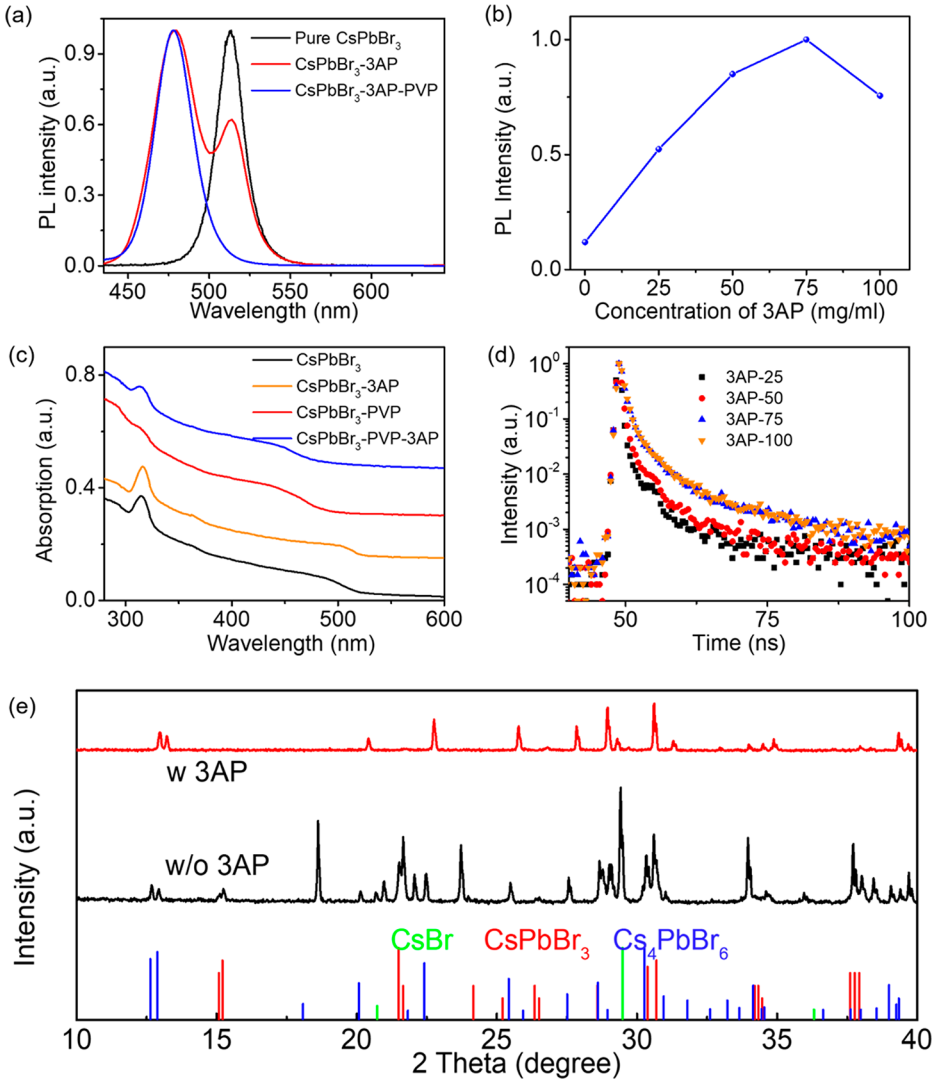


**Figure 1.** (a) Normalized spectra of the pure $CsPbBr_3$ formed on PEDOT:PSS with and without 3AP, as well as the PVP-$CsPbBr_3$ formed on 3AP-PEDOT:PSS. The pure $CsPbBr_3$ stands for the perovskite film without any additives. (b) PL intensity of the perovskite films on different concentrations of 3AP-doped PEDOT:PSS with a fixed PVP concentration of 10 mg/mL. (c) Absorption spectra for the perovskite films with different additives. (d) Transient PL decay curves for the PVP-$CsPbBr_3$ films on different concentrations of 3AP-doped PEDOT:PSS. (e) X-ray diffraction patterns for the perovskite with and without 3AP. The sample powders were fully ground by hand.

To date, inorganic materials have rarely been studied as spacers for constructing LD blue emissive perovskite films. In principle, ideal inorganic spacing layers are expected to have relatively larger electronic band gaps and lower dielectric constants than the perovskite layers to tune the energy band gap of the perovskite with large exciton binding energy.[26] In view of this point, optically transparent $Cs_4PbBr_6$ would be one of the possible inorganic spacers because it has a wider band gap (3.9 eV)[27] and lower dielectric constant[28] than $CsPbBr_3$. In addition, the $CsPbBr_3$:$Cs_4PbBr_6$ composite can be easily formed and adjusted by tuning the Cs/Pb ratio of the perovskite precursors. Such merit further endows the $Cs_4PbBr_6$ to be a promising inorganic spacer for $CsPbBr_3$. In fact, a blue shift has already been observed in the $CsPbBr_3$:$Cs_4PbBr_6$ composite because of the smaller domain size of $CsPbBr_3$ when more $Cs_4PbBr_6$ was incorporated in the composites.[29−32] However, such a blue shift is less than 10 nm, and blue emission has not yet been successfully observed. The main reason for the emission pinning in the green region is believed to be the nonuniform grain size of $CsPbBr_3$ resulting from the spontaneous crystallization process of $Cs_4PbBr_6$, which leads to the energy transfer from the larger band gap $CsPbBr_3$ nanoparticles to the narrower band gap $CsPbBr_3$ crystals.[30,31] Therefore, it is of great importance to regulate the crystallization of $Cs_4PbBr_6$ accurately to generate identical $Cs_4PbBr_6$ spaced $CsPbBr_3$ nanocomposites.

On the other hand, the thermal annealing process would promote the formation of the perovskite crystals,[33] resulting in further growth of the LD perovskites into the bulk phase.[34] This means that the as-prepared identical blue $CsPbBr_3$:$Cs_4PbBr_6$ composites may merge into large particles, resulting in a red shift of the spectra into green emission. Hence, another key point is to limit further growth of these $CsPbBr_3$:$Cs_4PbBr_6$ nanocomposites during the annealing process. A polymer matrix has been demonstrated to be an effective natural nanosized scaffold to impede the perovskite crystal growth.[35−40] However, an investigation of a polymer matrix on the growth and distribution of the $CsPbBr_3$:$Cs_4PbBr_6$ composites remains unexplored.


https://doi.org/10.1021/acsami.1c02555
ACS Appl. Mater. Interfaces 2021, 13, 33199−33208

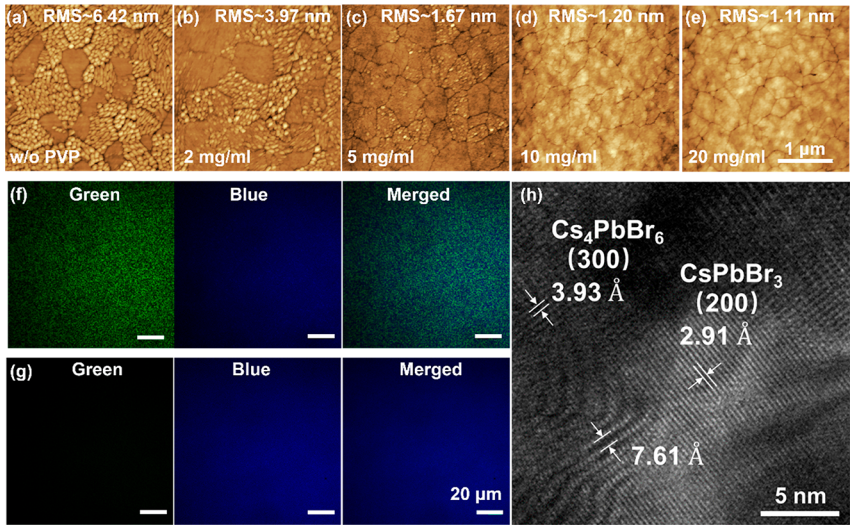


**Figure 2.** AFM images of perovskite films with different PVP's concentration: (a) without PVP, (b) 2 mg/mL, (c) 5 mg/mL, (d) 10 mg/mL, and (e) 20 mg/mL. (f) and (g) are the CLSM images corresponding to (a) and (d). The left images of (f) and (g) are obtained from the green channel ($\lambda_{ex}$ = 340 nm/$\lambda_{em}$ = 520 nm), the middle images are from the blue channel ($\lambda_{ex}$ = 340 nm/$\lambda_{em}$ = 480 nm), and the right images are merged images by summing the left and middle images. (h) High-resolution TEM images of the as-prepared perovskite films (PVP 10 mg/mL).

In this article, we demonstrate for the first time that inorganic $Cs_4PbBr_6$ could be used as a spacer to confine the $CsPbBr_3$ crystal to achieve blue emission. The blue emissive $CsPbBr_3$:$Cs_4PbBr_6$ nanocomposites were constructed through a 3-amino-1-propanol (3AP)-treated PEDOT:PSS (3AP-PEDOT:PSS) interfacial inducing strategy. More importantly, we reveal that tiny $CsPbBr_3$:$Cs_4PbBr_6$ nanostructures were well-retained by introducing PVP scaffold during the annealing process with high uniformity, resulting in an extremely smooth and stable blue emissive perovskite film. Consequently, efficient blue PeLED with electroluminescence centered at 485 nm has been demonstrated with a luminance of 2192 cd/m$^2$ and EQE of 2.3%. The device also exhibited superior operational stability with $T_{50}$ = 18.5 min, which was more than 3 times longer than that using long-chain organic spacers. These results highlight that the use of inorganic spacers might be a promising alternative route toward highly efficient and stable blue (bromide-based) PeLEDs.

## RESULTS AND DISCUSSION

For achievement of uniform $Cs_4PbBr_6$ spatially confined $CsPbBr_3$ nanocomposites, both the nucleation and crystallization have to be well controlled. Besides the control over the precursor stoichiometry and compositions, it has been demonstrated that the perovskite's crystallization can be significantly affected by the surface chemical and physical properties of the underlying interlayers during the perovskite crystallization process.[36,41−43] Therefore, here, we first implemented the amino and hydroxyl bifunctionalized 3AP to modify the hole transport layer (PEDOT:PSS) for stimulating the crystallization of $CsPbBr_3$:$Cs_4PbBr_6$ composites. The perovskite films were produced through a facile one-step spin-coating process. Briefly, the CsBr-rich perovskite precursor (CsBr and $PbBr_2$), either with or without PVP, was spun on the 3AP-PEDOT:PSS, followed by a low-temperature annealing at 70 °C (more details can be found in the Experimental Section). It is worth noting that the annealing temperature of 70 °C was optimized according to the maximum PLQY and the overall device performance (see Table S1). It is also found that the annealing temperature slightly influences the absorption properties as well as the crystal properties of the perovskite films (Figure S1). As shown in Figure 1a, the pure $CsPbBr_3$ film presented a single emission with a peak wavelength at ∼514 nm, which could be assigned to the bulk emission. In stark contrast, an additional peak at ∼478 nm appeared for the sample deposited on 3AP-doped PEDOT:PSS ($CsPbBr_3$−3AP), indicating that the film was composed by two different perovskite phases, which can be recognized by the surface morphology discussed below (Figure 2a). Clearly, the emission at 478 nm corresponding to the LD phase can be attributed to the 3AP's triggering role (illustrated in Figure S2), which may originate from the hydrogen bonding between −OH and Br atom as well as the amino terminal and $PbBr_6^{4-}$, as the Fourier transform infrared (FTIR) spectroscopy (Figure S3) revealed below. It is worth noting that no excitonic absorption signals for the LD domains were observed in the absorption spectrum for $CsPbBr_3$−3AP (Figure 1c), which may be shrouded by quasicontinuous absorptions, as reported in previous work.[44]

It should be mentioned that the $CsPbBr_3$−3AP film underwent a blue emissive state in the initial annealing process and gradually reached a cyan-blue state corresponding to a double-emission state after 5 min of annealing, as shown in Video S1. Such evolution suggests that the LD perovskite phases went through a growth process upon annealing. However, the initial blue state enlightened us in that a blue emission may be achieved if the growth process would be inhibited. Hence, we next attempted a polymer scaffold (PVP) into the perovskite film to suppress the growth of the LD phases. As shown in Figure 1a and Figure S4a, the bulk emission at 514 nm was gradually suppressed as the PVP doping concentration varied from 2 to 20 mg/mL. The emission peak center was fixed at 478 nm and the full width at half-maximum (fwhm) decreased to ∼27 nm as the PVP concentration exceeded 10 mg/mL. The transient absorption spectra showed only one ground state bleaching (GSB) peak located at around 460 nm (Figure S5), coinciding well with the absorption in the steady state. Such observations manifest that


https://doi.org/10.1021/acsami.1c02555
ACS Appl. Mater. Interfaces 2021, 13, 33199−33208

only one perovskite phase existed in the blue perovskite films, which is quite different from the organic-ligand spaced quasi-2D perovskites with multiphases. These results indicated an effective inhibition originating from the PVP scaffold for the growth of film from an LD phase into a bulk phase during thermal annealing. This spatial confinement role can also be verified by the prominent blue shift of the PL spectrum from ~514 to ~490 nm ($CsPbBr_3$−PVP sample) after the introduction of PVP additive (Figure S4b) as well as the weakened $Cs_4PbBr_6$ absorption peak at ~315 nm (Figure 1c).

To investigate whether the concentration of the 3AP in PEDOT:PSS would affect the PL characteristics of the LD phase, we measured the PL spectra of the perovskite films with different concentrations of 3AP at a fixed PVP concentration of 10 mg/mL. As shown in Figure 1b, the emission intensity showed an increased tendency as the 3AP concentration increased and achieved the maximum at a concentration of 75 mg/mL with a photoluminescence quantum yield of 15.8%. Time-resolved PL spectra were collected at a peak wavelength of 478 nm to further clarify the influence of the 3AP on the recombination kinetics in these films. As shown in Figure 1d, as the 3AP concentration increased from 25 to 100 mg/mL, the perovskite films exhibited slightly increased PL lifetimes ($\tau_{avg}$) with ~2.36, 2.77, 4.13, and 4.03 ns, respectively (see detailed fitting parameters in Table S2). Both the prolonged $\tau_{avg}$ and the increased PL intensity for the 3AP-75 perovskite sample revealed effective defect suppression that may arise from the passivation effect of 3AP-stimulated $Cs_4PbBr_6$[32,45] and the reduction of PEDOT:PSS caused PL quenching via lowering of its conductivity.[46] Intriguingly, it is found that the concentration of 3AP did not influence the LD emission peak center, as demonstrated by the PL spectra in Figure S4b. However, we found that the peak position was highly dependent on the Cs/Pb ratio ($x$) rather than the 3AP's and PVP's doping concentration. As shown in Figure S6 and Table S3, the PL peak can be flexibly tuned from 510 to 466 nm as $x$ changed from 1.4 to 1.95. Given that a larger Cs/Pb ratio would generate more $Cs_4PbBr_6$ and less $CsPbBr_3$, the blue-shifted PL spectra with increasing $x$ strongly unveiled that the $Cs_4PbBr_6$ played a decisive role in spatially confining the $CsPbBr_3$ crystal size. All in all, we have successfully realized blue emission LD $CsPbBr_3$ through the induction effect of 3AP on $CsPbBr_3$:$Cs_4PbBr_6$ composites and the restriction effect of PVP scaffold on their further growth.

To further demonstrate the triggering effect of 3AP on $Cs_4PbBr_6$, we measured the XRD for the perovskite powders ($x$ = 1.95) with and without 3AP additives (Figure 1e). For the perovskite film without 3AP, apart from the $CsPbBr_3$ and $Cs_4PbBr_6$ phases, an intense diffraction peak at $2\theta = 29.5°$ from CsBr was also observed. In stark contrast, after the introduction of 3AP, the diffraction peak intensity for CsBr and $CsPbBr_3$ ($2\theta = 15.2°$) decreased evidently, and the XRD peak for $Cs_4PbBr_6$ @ $2\theta = 22.4°$ increased accordingly. Meanwhile, FTIR spectroscopy was also measured to reveal the interaction between perovskite and 3AP (see Figure S3). In comparison to the pure 3AP, the characteristic band of −NH stretching modes (asymmetric stretching at 3353 $cm^{-1}$ and symmetric stretching at 3290 $cm^{-1}$) was greatly weakened, and a symmetric N−H umbrella band appeared in the 3AP−perovskite mixture, implying the existence of the protonated $-NH_3^+$ terminal group from the 3AP molecule. In addition, the absorption peak at 1372 $cm^{-1}$ belonging to the −OH group disappeared, indicating a removal of protons from the hydroxyl group, probably by forming hydrogen bonding of −OH···Br, as reported in a previous investigation.[47] The hydrogen bonding will facilitate the formation of $Cs_4PbBr_6$ under the CsBr-rich condition, as the XRD revealed, which also agrees well with the change of the absorption spectra (Figure 1c) where an increased $Cs_4PbBr_6$ absorption peak at ~315 nm was observed after the introduction of 3AP ($CsPbBr_3$−PVP−3AP sample).

For deeper insight into the PVP's influence on crystal growth, atomic force microscopy (AFM) was used to disclose the morphology evolution. As shown in Figure 2a, for a perovskite film without PVP, two completely different domains including a granuli-like and a big aggregates type can be observed. The roughness of the granuli-like domain was rather large, whereas the aggregated domain exhibited a very smooth surface, as confirmed by the corresponding 3D images in Figure S7. As the amount of PVP increased, the aggregates-like pieces increased, whereas the granuliform-composed domains reduced. Besides this change, the crystal size in the granuliform-composed domains also decreased, demonstrating that the PVP could impede the crystal growth effectively. When the PVP concentration reached 10 mg/mL, only aggregates-like domains existed in the perovskite film concomitant with a significantly decreased root-mean-square (RMS) of 1.2 nm. Such an extremely smooth and uniform morphology would be quite beneficial to the deposition of upper active layers and alleviate the unwanted shunting paths that cause nonradiative loss. Correlating the morphology evolution with the PL results (Figure 1a), we believe that the granulated crystals correspond to the bulk $CsPbBr_3$ and the big pieces were aggregated by small-size LD phases. To confirm our conjecture, we obtained fluorescent images of the perovskite films both with and without PVP (10 mg/mL) using confocal laser scanning microscopy (CLSM). For the sample without PVP, CLSM showed that, besides the green light-emission domains, blue spots also emerged and scattered in the films when detecting in the blue channel, as shown in Figure 2f. The merged image unambiguously confirmed that multicomponents coexisted in the perovskite film. In contrast, for the perovskite film with PVP (corresponding to the morphology in Figure 2d), only uniform blue emission could be observed (see Figure 2g). These observations demonstrated once again that the granulated crystals and the aggregates were the bulk green perovskite phases and LD blue phases, respectively, and the bulk phase could be completely suppressed under the interaction of PVP. Meanwhile, high-resolution transmission electron microscopy (HRTEM) image (Figure 2h) of the films with PVP showed that the lattice spacings were 2.91 and 3.93 Å, which corresponded well to the (200) planes of the $CsPbBr_3$ phase and (300) planes of $Cs_4PbBr_6$, respectively. A Moiré fringe pattern (7.61 ± 0.1 Å) was also observed, which may result from the overlapping of the (220) plane of $Cs_4PbBr_6$ and (200) plane of $CsPbBr_3$ according to the following equation:

$$d_{(\text{Moire}')} = \frac{d_{200}^2}{2(d_{220} - d_{200})} = 7.70 \pm 0.1 \text{ Å} \quad (1)$$

These results coincided well with the absorption results and confirmed that the blue emission originated from the $CsPbBr_3$:$Cs_4PbBr_6$ nanocomposites. The above results clearly demonstrate that PVP could facilitate the dispersion of the $CsPbBr_3$:$Cs_4PbBr_6$ nanocomposites and impede their growth


https://doi.org/10.1021/acsami.1c02555
ACS Appl. Mater. Interfaces 2021, 13, 33199−33208

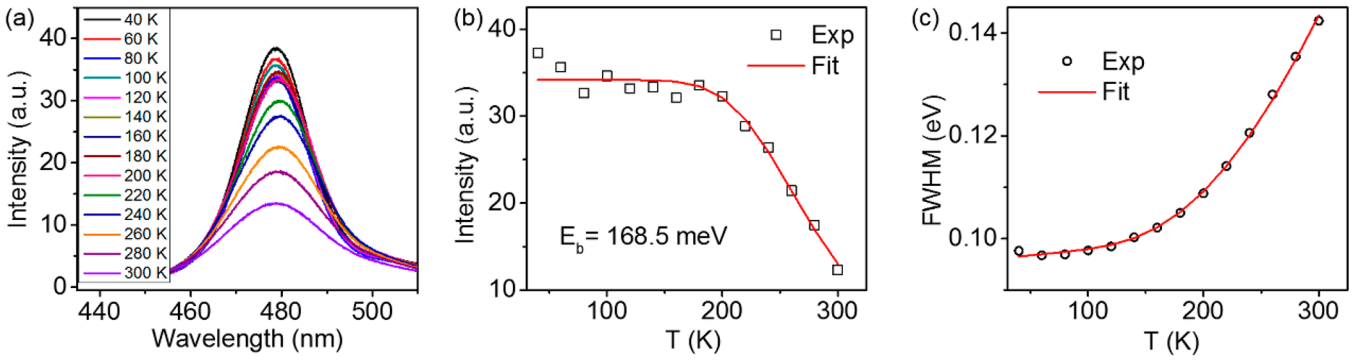


**Figure 3.** Temperature-dependent (a) PL spectra, (b) PL intensity, and (c) fwhm of the as-prepared perovskite film with both 3AP (75 mg/mL) and PVP (10 mg/mL) as the temperature varied from 40 to 300 K with an interval of 20 K.

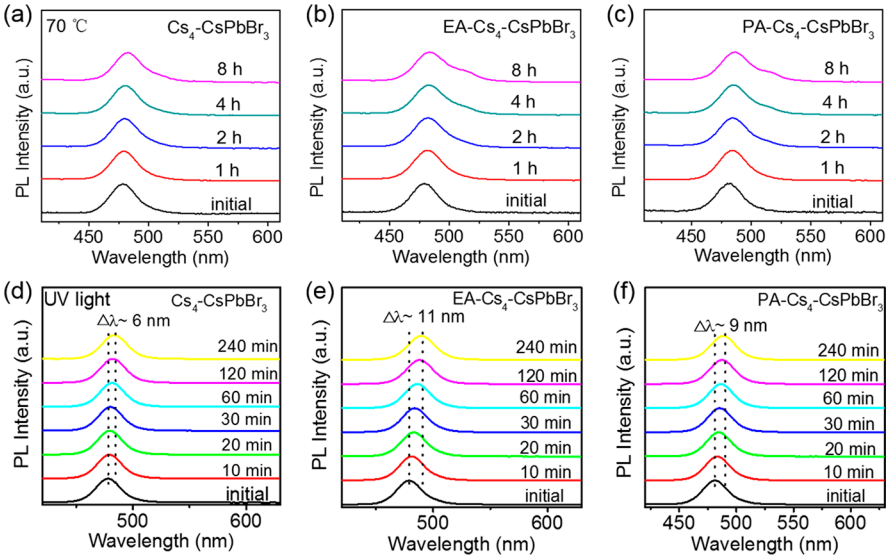


**Figure 4.** Thermal and UV stability of the perovskite films with a $Cs_4PbBr_6$ spacer (a, d), an EA–$Cs_4PbBr_6$ coexisting spacer (b, e), and a PA–$Cs_4PbBr_6$ coexisted spacer (c, f), respectively.

upon heating, as illustrated in Figure S2, which was a key additive for the realization of the ultrasmooth blue emissive perovskite films.

For acquisition of more intrinsic characteristics of the exciton in the blue emissive perovskite films, a temperature-dependent PL measurement was performed in a continuous helium flowed cryostat. As displayed in Figure 3a, the PL intensity gradually decreased with increasing temperature from 40 to 300 K, indicating a thermal quenching of the PL emission. The key physical parameter of the exciton binding energy ($E_b$), which closely relates to the charge transfer and exciton dissociation probability in the PL process, could be extracted by fitting the PL intensities using the following Arrhenius equation:[48]

$$I(T) = I_0 / \left(1 + A \exp\left(-\frac{E_b}{k_B T}\right)\right) \quad (2)$$

where $I_0$ denotes the initial PL intensity and $k_B$ represents the Boltzmann's constant. The $E_b$ for the blue perovskite film was as large as 168.5 meV thanks to the synergetic confinement of PVP and $Cs_4PbBr_6$. This value was much larger than that of the bulk $CsPbBr_3$ materials with an $E_b$ of 65.45 meV (shown in Figure S8) as well as the room-temperature thermal disturbance energy (~26 meV), which would contribute efficient exciton generation and recombination, which is desired for the EL devices. The PL peak (band gap) from 40 to 300 K is almost independent of the temperature with a peak shift of less than 1 nm (Figure S9). Previous reports revealed that the band gap evolution with temperature hinged on the species of the organic spacers and layer number $n$.[49,50] The former usually causes a band gap red shift because of the exciton–phonon interaction, whereas the latter causes a band gap blue shift as a result of the thermal expansion effect. Here, in our case, the red shift caused by exciton–phonon interactions and a blue shift caused by the thermal expansion effect are believed to be comparable and thus cancel each other out.

With further analysis of the line widths evolution under different temperatures, a deep understanding of the exciton–phonon coupling could be obtained. Figure 3c showed the relationship between fwhm and the temperature. The exciton–phonon coupling is considered to be relevant to acoustic phonon scattering and longitudinal optical (LO) phonon scattering and can be well described by the following equation:[51,52]

$$\Gamma(T) = \Gamma_{inh} + \gamma_{ac} T + \gamma_{LO} / (e^{E_{LO}/k_B T} - 1) \quad (3)$$



https://doi.org/10.1021/acsami.1c02555
ACS Appl. Mater. Interfaces 2021, 13, 33199–33208

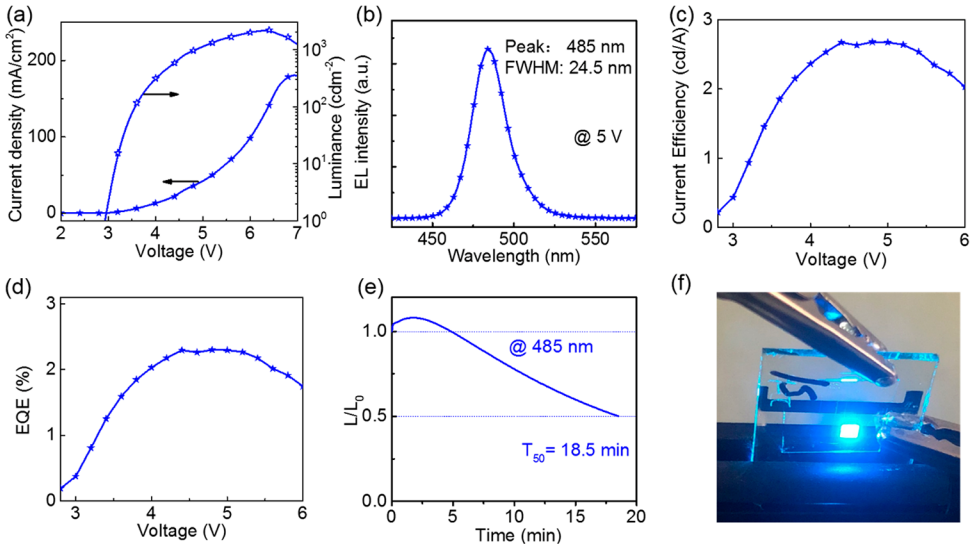


**Figure 5.** Electroluminescent performance for the PeLEDs with fixed concentrations of 3AP-PEDOT:PSS (75 mg/mL) and PVP (10 mg/mL). (a) Current density and luminance curves as a function of driven voltage. (b) Normalized spectra of the PeLEDs at 5 V. (c) Current efficiency curves. (d) EQE curves as a function of driven voltage. (e) Operational stability of the PeLEDs with emission @ 485 nm driven under a continuous constant current density with an initial luminance of 100 cd/m$^2$. (f) Optical image of a working PeLED.

where $\Gamma_{inh}$ is the temperature-independent inhomogeneous broadening contribution. $\gamma_{ac}$ and $\gamma_{LO}$ are the acoustic and LO phonon coupling coefficient, respectively. $E_{LO}$ is the average optical phonon energy. The well-fitted results demonstrate that the line width mainly presented linear increasing because of the dominating acoustic phonon scattering at low temperature (<140 K for both the $CsPbBr_3$ as well as the $CsPbBr_3$–3AP–PVP film (see Figure S8)) and superlinear broadening caused by LO phonon scattering at a higher temperature (>140 K) or even room temperature. Such observations were similar to exciton–phonon coupling in other quasi-2D cesium lead bromide perovskites.[53]

We next investigated the color stability of the inorganic $Cs_4PbBr_6$ spacer based blue perovskite films. For a better comparison, we replaced partial $Cs_4PbBr_6$ with the organic spacer ethylammonium (EA) and propylammonium (PA) to fabricate the blue perovskite films with almost the same emission peak. These samples were labeled as $Cs_4$–$CsPbBr_3$, EA–$Cs_4$–$CsPbBr_3$, and PA–$Cs_4$–$CsPbBr_3$, respectively. Aging tests under continuous heating at 70 °C or UV excitation by 365 nm (1 W cm$^{-2}$) were carried out on these blue perovskite films. The evolution of the emission properties are presented in Figure 4. After 8 h of heat aging, the PL spectra profiles were almost unchanged for the $Cs_4$–$CsPbBr_3$ film. In contrast, the spectra for the EA–$Cs_4$–$CsPbBr_3$ film and PA–$Cs_4$–$CsPbBr_3$ film exhibited an unintended shoulder peak at a longer wavelength (around ∼514 nm) after about 4 h of heating. The additional peak probably arose from the regrowth of the small $CsPbBr_3$. Such a change in the spectra demonstrated that the $CsPbBr_3$ film with a $Cs_4PbBr_6$ spacer could bear better resistance to heat than that with the organic spacers, which may be further beneficial to the operational stability of the PeLEDs. Figure 4d–f showed spectra stability under UV excitation. All the samples exhibited a red shift against UV illumination, which was similar to those in a previous investigation.[43] However, there is only a 6 nm red shift for the $Cs_4$–$CsPbBr_3$ after 240 min of UV illumination, which is less than that for EA–$Cs_4$–$CsPbBr_3$ film (11 nm) and PA–$Cs_4$–$CsPbBr_3$ film (9 nm). These results manifest that the $Cs_4PbBr_6$ would be an effective inorganic spacer to construct the blue Cs-based perovskite films with superior stability, which may be conducive to the operational stability of the blue PeLEDs.

Inspired by the ultrasmooth morphology and the color-stable characteristics of these perovskite films, we further fabricated the PeLEDs with a structure of ITO/3AP–PEDOT:PSS/perovskite/TPBI/LiF/Al (see more details in the Experimental Section and Figure S10a). Apart from inducing the $CsPbBr_3$:$Cs_4PbBr_6$ nanocomposite, the 3AP could also enhance the hole transport from the HTL to the EML by deepening the work function of the PEDOT:PSS. The 3AP-PEDOT:PSS hole transport layer exhibited a deeper work function of ∼5.41 eV,[46] compared to the pure PEDOT:PSS (5.01 eV),[54] as shown in Figure S10b, which would be conductive to the hole injection from the HTL into the perovskite EML. TPBI was adopted as the electron transport layer. LiF was used as the electron injection layer. The performance of the PeLEDs are displayed in Figure 5, and related parameters are summarized in Table S3. Benefiting from the dense morphology, the leakage current of the device was well suppressed below $10^{-2}$ mA/cm$^2$, as shown in Figure S11a. The blue device presented good color purity with an EL peak at 485 nm and a fwhm of 24.5 nm. The red shift in EL spectra in comparison to that of the PL spectra could originate from a carrier trapping process by the lower band gap components in the films.[29] The corresponding color coordinates of the International Commission on Illumination (CIE) were (0.08, 0.23). The blue PeLED achieved a maximum luminance of 2192 cd/m$^2$, a current efficiency of 2.68 cd/A, and an EQE of 2.3%. Moreover, consistent with the PL spectra, the EL spectra (Figure S11b) can also be flexibly modulated from 512 to 474 nm with high color purities (fwhm of 20.5 ($x$ = 1.4), 23.7 ($x$ = 1.55), 24.4 ($x$ = 1.71), 24.5 ($x$ = 1.86), and 30.9 nm ($x$ = 1.95), respectively), as presented in Figure S11b and Table S3. The operational lifetime ($T_{50}$ @ 100 cd/m$^2$) under a constant current density reached up to 18.5 min PeLED @ 485 nm (Figure 5e). Such working stability was greatly enhanced, in stark contrast to the devices


https://doi.org/10.1021/acsami.1c02555
ACS Appl. Mater. Interfaces 2021, 13, 33199–33208

that implemented the organic spacers of EA and PA, which survived only for 5.7 and 3.9 min, respectively (see Figure S12). It should be mentioned that, among the reported $CsPbBr_3$ based blue PeLEDs, the working stability for our devices was also superior compared to those using long-chain organic spacers (see Table S4). We believe the superior conductivity arising from $Cs_4PbBr_6$ compared to that of the organic long-chain spacers may play a critical role. To better demonstrate the improvement of conductivity of the perovskite layer, we fabricated a group of hole-only devices. As shown in Figure S13, the $Cs_4PbBr_6$−$CsPbBr_3$ film exhibited a higher current density compared to the EA−$CsPbBr_3$ film, confirming that better conductivity would be achieved when using $Cs_4PbBr_6$ as a spacer. The bright blue PeLEDs (Figure 5f) also presented exceptional spectra stability with almost no peak shift, both under a continuously driven current at a fixed voltage of 5 V and an increased voltage from 3.0 to 6.5 V (Figure S14). This manifested that the blue emissive $CsPbBr_3$ LD perovskite was very stable under both thermal heating and an electrical field, again highlighting the merits of the inorganic spacer of $Cs_4PbBr_6$.

## CONCLUSION

In summary, we have demonstrated blue emission in an inorganic $Cs_4PbBr_6$ spaced low-dimensional $CsPbBr_3$. 3AP tailored PEDOT:PSS can trigger the formation and distribution of $Cs_4PbBr_6$ perovskite phase to facilitate the formation of LD $CsPbBr_3$:$Cs_4PbBr_6$. PVP can act as a polymer scaffold to further suppress the appearance of bulk phase to achieve uniformly distributed LD perovskite films with an ultrasmooth surface morphology (rms of ∼1.2 nm). With this novel strategy, efficient green-to-blue PeLEDs with EL from 512 to 474 nm were realized. Compared to the blue perovskite films using organic spacers, the all-inorganic $Cs_4PbBr_6$ spacer endows the LD perovskite phase with higher color stability against heat and UV excitation. Especially, blue PeLEDs at a wavelength of 485 nm exhibited a brightness of 2192 cd/m$^2$, CE of 2.68 cd/A, EQE of 2.3%, and a lifetime of 18.5 min. Our results will serve as an alternative strategy to construct stable blue PeLEDs.

## EXPERIMENTAL SECTION

**Materials.** PEDOT:PSS (Clevios, AI4083), $PbBr_2$ (99.9%), and 1,3,5-tris(2-*N*-phenylbenzimidazolyl)-benzene (TPBi) were purchased from Xi'an Polymer Light Technology Corp. CsBr (99.9%) was purchased from Kanto Chemical. Co., Inc. LiF (99.99%), 3-amino-1-propanol (3AP), and PVP ($M_w$ = 1 300 000) were purchased from Aladdin.

**Film Fabrication and Characterization.** The 3AP-doped PEDOT:PSS and perovskite precursor were prepared as reported in our earlier work.[46] The PVP was dissolved in DMSO with desired weight concentrations. The perovskite precursor and the PVP solution were blended at a volume ratio of 10:1 before use. For the samples with organic spacers, additional EABr or PABr was introduced into the precursor (Cs/Pb ratio of 1.6) with a concentration of 20 mg/mL. The morphology of the perovskite films was characterized by AFM (Shimadzu SPA-9700). The PL spectra were recorded by a fluorescence spectrometer (Hitachi F-7000) with an excitation wavelength of 400 nm. Time-resolved PL spectra were analyzed with an Edinburgh FLS920 spectrometer. Absorption spectra of perovskite film were characterized by a Persee T6 UV−vis spectrometer. Temperature-dependent PL spectra were collected using a Horiba iHR550 system equipped with 405 nm solid-state lasers and a helium-follow cryostat. CLSM was performed using a Nikon Eclipse Ti2 microscope. The XRD patterns of perovskite powders obtained by hand grinding were carried out by Rigaku SmartLab. The FTIR was measured on a Thermo-Nicole iS50 FTIR-spectrometer.

**Device Fabrication and Characterization.** The ITO substrates were cleaned with deionized water, ethanol, and acetone solvents successively and then treated under an UV-ozone environment for 20 min. Then the 3AP−PEDOT:PSS was spin-coated on ITO substrates at 2500 rpm for 45 s and annealed at 140 °C for 20 min. Then the substrates were transferred into a nitrogen-filled glovebox to prepare the perovskite layer. Subsequently, the samples were transferred into a homemade vacuum chamber (QHV-R20) to thermally deposit the following TPBi (40 nm), LiF (2 nm), and Al (100 nm) under a pressure of below $4 \times 10^{-4}$ Pa. The effective area of the PeLED was 0.08 cm$^2$. The PeLED's brightness and current density were measured using a Keithley 2400 source meter coupled with a luminance meter LS160. The EL spectra were recorded with an AvaSpec-ULS2048L fiber spectrometer. A Lambertian emission profile was assumed in calculating the EQE from the brightness, current, and EL spectrum. All measurements were performed in air with simple encapsulation by UV glue.

## ASSOCIATED CONTENT

### Supporting Information

The Supporting Information is available free of charge at https://pubs.acs.org/doi/10.1021/acsami.1c02555.

Video S1 (AVI)

Transient absorption, PL, and EL curves; 3D AFM images; peak centers versus temperature; device structure and EL performance of the PeLED (PDF)

## AUTHOR INFORMATION


### Corresponding Authors

**Li Song** − *State Key Laboratory of Reliability and Intelligence of Electrical Equipment and Tianjin Key Laboratory of Electronic Materials and Devices, School of Electronics and Information Engineering, Hebei University of Technology, Tianjin 300401, P.R. China*; orcid.org/0000-0002-4781-4023; Email: songli@hebut.edu.cn

**Yongsheng Hu** − *School of Physics and Microelectronics, Zhengzhou University, Zhengzhou 450001, China*; Email: h0y0s@163.com

**Xiaoyang Guo** − *State Key Laboratory of Luminescence and Applications, Changchun Institute of Optics, Fine Mechanics and Physics, Chinese Academy of Sciences, Changchun 130033, China*; orcid.org/0000-0003-0259-137X; Email: guoxy@ciomp.ac.cn

### Authors

**Lixin Huang** − *State Key Laboratory of Reliability and Intelligence of Electrical Equipment and Tianjin Key Laboratory of Electronic Materials and Devices, School of Electronics and Information Engineering, Hebei University of Technology, Tianjin 300401, P.R. China*

**Yuan Liu** − *State Key Laboratory of Reliability and Intelligence of Electrical Equipment and Tianjin Key Laboratory of Electronic Materials and Devices, School of Electronics and Information Engineering, Hebei University of Technology, Tianjin 300401, P.R. China*

**Yulei Chang** − *State Key Laboratory of Luminescence and Applications, Changchun Institute of Optics, Fine Mechanics and Physics, Chinese Academy of Sciences, Changchun 130033, China*; orcid.org/0000-0001-7223-1797

**Chong Geng** − *State Key Laboratory of Reliability and Intelligence of Electrical Equipment and Tianjin Key*

*Laboratory of Electronic Materials and Devices, School of Electronics and Information Engineering, Hebei University of Technology, Tianjin 300401, P.R. China;* orcid.org/0000-0002-7200-6394

**Shu Xu** − *State Key Laboratory of Reliability and Intelligence of Electrical Equipment and Tianjin Key Laboratory of Electronic Materials and Devices, School of Electronics and Information Engineering, Hebei University of Technology, Tianjin 300401, P.R. China;* orcid.org/0000-0002-4185-1392

**Zihui Zhang** − *State Key Laboratory of Reliability and Intelligence of Electrical Equipment and Tianjin Key Laboratory of Electronic Materials and Devices, School of Electronics and Information Engineering, Hebei University of Technology, Tianjin 300401, P.R. China;* orcid.org/0000-0003-0638-1118

**Yonghui Zhang** − *State Key Laboratory of Reliability and Intelligence of Electrical Equipment and Tianjin Key Laboratory of Electronic Materials and Devices, School of Electronics and Information Engineering, Hebei University of Technology, Tianjin 300401, P.R. China*

**Nannan Luan** − *State Key Laboratory of Reliability and Intelligence of Electrical Equipment and Tianjin Key Laboratory of Electronic Materials and Devices, School of Electronics and Information Engineering, Hebei University of Technology, Tianjin 300401, P.R. China*

Complete contact information is available at: https://pubs.acs.org/10.1021/acsami.1c02555

### Notes

The authors declare no competing financial interest.

## ■ ACKNOWLEDGMENTS

This study was supported by the Natural Science Foundation of Hebei Province (F2019202252, F2019202294), the State Key Laboratory of Luminescence and Applications (SKLA-2019-07), the National Natural Science Foundation of China (No. 61774154, 51902082, 61975256, 51973280, 62035013, 11904323), and State Key Laboratory of Reliability and Intelligence of Electrical Equipment, Hebei University of Technology (No. EERI_PI2020008).

## ■ REFERENCES

(1) Miao, Y.; Cheng, L.; Zou, W.; Gu, L.; Zhang, J.; Guo, Q.; Peng, Q.; Xu, M.; He, Y.; Zhang, S.; Cao, Y.; Li, R.; Wang, N.; Huang, W.; Wang, J. Microcavity Top-Emission Perovskite Light-Emitting Diodes. *Light: Sci. Appl.* **2020**, *9*, 89.

(2) Kang, C. H.; Dursun, I.; Liu, G.; Sinatra, L.; Sun, X.; Kong, M.; Pan, J.; Maity, P.; Ooi, E.-N.; Ng, T. K.; Mohammed, O. F.; Bakr, O. M.; Ooi, B. S. High-Speed Colour-Converting Photodetector with All-Inorganic $CsPbBr_3$ Perovskite Nanocrystals for Ultraviolet Light Communication. *Light: Sci. Appl.* **2019**, *8*, 94.

(3) Chang, S.; Bai, Z.; Zhong, H. In Situ Fabricated Perovskite Nanocrystals: A Revolution in Optical Materials. *Adv. Opt. Mater.* **2018**, *6*, 1800380.

(4) Cao, Y.; Wang, N.; Tian, H.; Guo, J.; Wei, Y.; Chen, H.; Miao, Y.; Zou, W.; Pan, K.; He, Y.; Cao, H.; Ke, Y.; Xu, M.; Wang, Y.; Yang, M.; Du, K.; Fu, Z.; Kong, D.; Dai, D.; Jin, Y.; Li, G.; Li, H.; Peng, Q.; Wang, J.; Huang, W. Perovskite Light-Emitting Diodes Based on Spontaneously Formed Submicrometre-Scale Structures. *Nature* **2018**, *562*, 249−253.

(5) Lin, K.; Xing, J.; Quan, L. N.; de Arquer, F. P. G.; Gong, X.; Lu, J.; Xie, L.; Zhao, W.; Zhang, D.; Yan, C.; Li, W.; Liu, X.; Lu, Y.; Kirman, J.; Sargent, E. H.; Xiong, Q.; Wei, Z. Perovskite Light-Emitting Diodes with External Quantum Efficiency Exceeding 20%. *Nature* **2018**, *562*, 245−248.

(6) Chiba, T.; Hayashi, Y.; Ebe, H.; Hoshi, K.; Sato, J.; Sato, S.; Pu, Y.-J.; Ohisa, S.; Kido, J. Anion-Exchange Red Perovskite Quantum Dots with Ammonium Iodine Salts for Highly Efficient Light-Emitting Devices. *Nat. Photonics* **2018**, *12*, 681−687.

(7) Xu, W. D.; Hu, Q.; Bai, S.; Bao, C. X.; Miao, Y. F.; Yuan, Z. C.; Borzda, T.; Barker, A. J.; Tyukalova, E.; Hu, Z. J.; Kawecki, M.; Wang, H. Y.; Yan, Z. B.; Liu, X. J.; Shi, X. B.; Uvdal, K.; Fahlman, M.; Zhang, W. J.; Duchamp, M.; Liu, J. M.; Petrozza, A.; Wang, J. P.; Liu, L. M.; Huang, W.; Gao, F. Rational Molecular Passivation for High-Performance Perovskite Light-Emitting Diodes. *Nat. Photonics* **2019**, *13*, 418−424.

(8) Zhao, B.; Bai, S.; Kim, V.; Lamboll, R.; Shivanna, R.; Auras, F.; Richter, J. M.; Yang, L.; Dai, L.; Alsari, M.; She, X.-J.; Liang, L.; Zhang, J.; Lilliu, S.; Gao, P.; Snaith, H. J.; Wang, J.; Greenham, N. C.; Friend, R. H.; Di, D. High-Efficiency Perovskite-Polymer Bulk Heterostructure Light-Emitting Diodes. *Nat. Photonics* **2018**, *12*, 783−800.

(9) Hassan, Y.; Park, J. H.; Crawford, M. L.; Sadhanala, A.; Lee, J.; Sadighian, J. C.; Mosconi, E.; Shivanna, R.; Radicchi, E.; Jeong, M.; Yang, C.; Choi, H.; Park, S. H.; Song, M. H.; De Angelis, F.; Wong, C. Y.; Friend, R. H.; Lee, B. R.; Snaith, H. J. Ligand-Engineered Bandgap Stability in Mixed-Halide Perovskite LEDs. *Nature* **2021**, *591*, 72−77.

(10) Kim, Y. H.; Kim, S.; Kakekhani, A.; Park, J.; Park, J.; Lee, Y. H.; Xu, H. X.; Nagane, S.; Wexler, R. B.; Kim, D. H.; Jo, S. H.; Martinez-Sarti, L.; Tan, P.; Sadhanala, A.; Park, G. S.; Kim, Y. W.; Hu, B.; Bolink, H. J.; Yoo, S.; Friend, R. H.; Rappe, A. M.; Lee, T. W. Comprehensive Defect Suppression in Perovskite Nanocrystals for High-Efficiency Light-Emitting Diodes. *Nat. Photonics* **2021**, *15*, 148−155.

(11) Xing, J.; Zhao, Y.; Askerka, M.; Quan, L. N.; Gong, X.; Zhao, W.; Zhao, J.; Tan, H.; Long, G.; Gao, L.; Yang, Z.; Voznyy, O.; Tang, J.; Lu, Z.-H.; Xiong, Q.; Sargent, E. H. Color-Stable Highly Luminescent Sky-Blue Perovskite Light-Emitting Diodes. *Nat. Commun.* **2018**, *9*, 3541.

(12) Hou, S.; Gangishetty, M. K.; Quan, Q.; Congreve, D. N. Efficient Blue and White Perovskite Light-Emitting Diodes Via Manganese Doping. *Joule* **2018**, *2*, 2421−2433.

(13) Vashishtha, P.; Ng, M.; Shivarudraiah, S. B.; Halpert, J. E. High Efficiency Blue and Green Light-Emitting Diodes Using Ruddlesden−Popper Inorganic Mixed Halide Perovskites with Butylammonium Interlayers. *Chem. Mater.* **2019**, *31*, 83−89.

(14) Braly, I. L.; Stoddard, R. J.; Rajagopal, A.; Uhl, A. R.; Katahara, J. K.; Jen, A. K. Y.; Hillhouse, H. W. Current-Induced Phase Segregation in Mixed Halide Hybrid Perovskites and Its Impact on Two-Terminal Tandem Solar Cell Design. *ACS Energy Lett.* **2017**, *2*, 1841−1847.

(15) Li, G.; Rivarola, F. W. R.; Davis, N. J. L. K.; Bai, S.; Jellicoe, T. C.; de la Peña, F.; Hou, S.; Ducati, C.; Gao, F.; Friend, R. H.; Greenham, N. C.; Tan, Z.-K. Highly Efficient Perovskite Nanocrystal Light-Emitting Diodes Enabled by a Universal Crosslinking Method. *Adv. Mater.* **2016**, *28*, 3528−3534.

(16) Chu, Z.; Zhao, Y.; Ma, F.; Zhang, C.-X.; Deng, H.; Gao, F.; Ye, Q.; Meng, J.; Yin, Z.; Zhang, X.; You, J. Large Cation Ethylammonium Incorporated Perovskite for Efficient and Spectra Stable Blue Light-Emitting Diodes. *Nat. Commun.* **2020**, *11*, 4165.

(17) Liu, Y.; Cui, J.; Du, K.; Tian, H.; He, Z.; Zhou, Q.; Yang, Z.; Deng, Y.; Chen, D.; Zuo, X.; Ren, Y.; Wang, L.; Zhu, H.; Zhao, B.; Di, D.; Wang, J.; Friend, R. H.; Jin, Y. Efficient Blue Light-Emitting Diodes Based on Quantum-Confined Bromide Perovskite Nanostructures. *Nat. Photonics* **2019**, *13*, 760−764.

(18) Ren, Z. W.; Li, L.; Yu, J. H.; Ma, R. M.; Xiao, X. T.; Chen, R.; Wang, K.; Sun, X. W.; Yin, W. J.; Choy, W. C. H. Simultaneous Low-Order Phase Suppression and Defect Passivation for Efficient and Stable Blue Light-Emitting Diodes. *ACS Energy Lett.* **2020**, *5*, 2569−2579.

(19) Zou, Y.; Xu, H.; Li, S.; Song, T.; Kuai, L.; Bai, S.; Gao, F.; Sun, B. Spectral-Stable Blue Emission from Moisture-Treated Low-

Dimensional Lead Bromide-Based Perovskite Films. *ACS Photonics* **2019**, *6*, 1728−1735.
(20) Ren, Z.; Xiao, X.; Ma, R.; Lin, H.; Wang, K.; Sun, X. W.; Choy, W. C. H. Hole Transport Bilayer Structure for Quasi-2D Perovskite Based Blue Light-Emitting Diodes with High Brightness and Good Spectral Stability. *Adv. Funct. Mater.* **2019**, *29*, 1905339.
(21) Zhang, F. J.; Cai, B.; Song, J. Z.; Han, B. N.; Zhang, B. S.; Zeng, H. B. Efficient Blue Perovskite Light-Emitting Diodes Boosted by 2D/3D Energy Cascade Channels. *Adv. Funct. Mater.* **2020**, *30*, 2001732.
(22) Zeng, S. Y.; Shi, S. S.; Wang, S. R.; Xiao, Y. Mixed-Ligand Engineering of Quasi-2D Perovskites for Efficient Sky-Blue Light-Emitting Diodes. *J. Mater. Chem. C* **2020**, *8*, 1319−1325.
(23) Worku, M.; He, Q. Q.; Xu, L. J.; Hong, J.; Yang, R. X.; Tan, L.; Ma, B. W. Phase Control and in Situ Passivation of Quasi-2D Metal Halide Perovskites for Spectrally Stable Blue Light-Emitting Diodes. *ACS Appl. Mater. Interfaces* **2020**, *12*, 45056−45063.
(24) Zhang, F.; Kim, D. H.; Lu, H.; Park, J.-S.; Larson, B.; Hu, J.; Gao, L.; Xiao, C.; Reid, O.; Chen, X.; Zhao, Q.; Ndione, P. F.; Berry, J. J.; You, W.; Walsh, A.; Beard, M. C.; Zhu, K. Enhanced Charge Transport in 2D Perovskite Via Fluorination of Organic Cation. *J. Am. Chem. Soc.* **2019**, *141*, 5972−5979.
(25) Wu, T.; Li, J. N.; Zou, Y. T.; Xu, H.; Wen, K. C.; Wan, S. S.; Bai, S.; Song, T.; McLeod, J. A.; Duhm, S.; Gao, F.; Sun, B. Q. High-Performance Perovskite Light-Emitting Diode with Enhanced Operational Stability Using Lithium Halide Passivation. *Angew. Chem., Int. Ed.* **2020**, *59*, 4099−4105.
(26) Straus, D. B.; Kagan, C. R. Electrons, Excitons, and Phonons in Two-Dimensional Hybrid Perovskites: Connecting Structural, Optical, and Electronic Properties. *J. Phys. Chem. Lett.* **2018**, *9*, 1434−1447.
(27) Wang, L.; Liu, H.; Zhang, Y.; Mohammed, O. F. Photoluminescence Origin of Zero-Dimensional $Cs_4PbBr_6$ Perovskite. *ACS Energy Lett.* **2020**, *5*, 87−99.
(28) Kang, B.; Biswas, K. Exploring Polaronic, Excitonic Structures and Luminescence in $Cs_4PbBr_6$/$CsPbBr_3$. *J. Phys. Chem. Lett.* **2018**, *9*, 830−836.
(29) Shang, Y. Q.; Li, G.; Liu, W. M.; Ning, Z. J. Quasi-2D Inorganic $CsPbBr_3$ Perovskite for Efficient and Stable Light-Emitting Diodes. *Adv. Funct. Mater.* **2018**, *28*, 1801193.
(30) Xu, J.; Huang, W.; Li, P.; Onken, D. R.; Dun, C.; Guo, Y.; Ucer, K. B.; Lu, C.; Wang, H.; Geyer, S. M.; Williams, R. T.; Carroll, D. L. Imbedded Nanocrystals of $CsPbBr_3$ in $Cs_4PbBr_6$: Kinetics, Enhanced Oscillator Strength, and Application in Light-Emitting. *Adv. Mater.* **2017**, *29*, 1703703.
(31) Quan, L. N.; Quintero-Bermudez, R.; Voznyy, O.; Walters, G.; Jain, A.; Fan, J. Z.; Zheng, X.; Yang, Z.; Sargent, E. H. Highly Emissive Green Perovskite Nanocrystals in a Solid State Crystalline Matrix. *Adv. Mater.* **2017**, *29*, 1605945.
(32) Ling, Y.; Tan, L.; Wang, X.; Zhou, Y.; Xin, Y.; Ma, B.; Hanson, K.; Gao, H. Composite Perovskites of Cesium Lead Bromide for Optimized Photoluminescence. *J. Phys. Chem. Lett.* **2017**, *8*, 3266−3271.
(33) Yu, J. C.; Kim, D. W.; Kim, D. B.; Jung, E. D.; Park, J. H.; Lee, A.-Y.; Lee, B. R.; Di Nuzzo, D.; Friend, R. H.; Song, M. H. Improving the Stability and Performance of Perovskite Light-Emitting Diodes by Thermal Annealing Treatment. *Adv. Mater.* **2016**, *28*, 6906−6913.
(34) Zhou, N.; Shen, Y.; Li, L.; Tan, S.; Liu, N.; Zheng, G.; Chen, Q.; Zhou, H. Exploration of Crystallization Kinetics in Quasi Two-Dimensional Perovskite and High Performance Solar Cells. *J. Am. Chem. Soc.* **2018**, *140*, 459−465.
(35) Ling, Y.; Tian, Y.; Wang, X.; Wang, J. C.; Knox, J. M.; Perez-Orive, F.; Du, Y.; Tan, L.; Hanson, K.; Ma, B.; Gao, H. Enhanced Optical and Electrical Properties of Polymer-Assisted All-Inorganic Perovskites for Light-Emitting Diodes. *Adv. Mater.* **2016**, *28*, 8983−8989.
(36) Cho, H.; Wolf, C.; Kim, J. S.; Yun, H. J.; Bae, J. S.; Kim, H.; Heo, J.-M.; Ahn, S.; Lee, T.-W. High-Efficiency Solution-Processed Inorganic Metal Halide Perovskite Light-Emitting Diodes. *Adv. Mater.* **2017**, *29*, 1700579.
(37) Li, J.; Shan, X.; Bade, S. G. R.; Geske, T.; Jiang, Q.; Yang, X.; Yu, Z. Single-Layer Halide Perovskite Light-Emitting Diodes with Sub-Band Gap Turn-on Voltage and High Brightness. *J. Phys. Chem. Lett.* **2016**, *7*, 4059−4066.
(38) Lin, H.; Zhu, L.; Huang, H.; Reckmeier, C. J.; Liang, C.; Rogach, A. L.; Choy, W. C. H. Efficient near-Infrared Light-Emitting Diodes Based on Organometallic Halide Perovskite-Poly(2-Ethyl-2-Oxazoline) Nanocomposite Thin Films. *Nanoscale* **2016**, *8*, 19846−19852.
(39) Song, L.; Guo, X.; Hu, Y.; Lv, Y.; Lin, J.; Liu, Z.; Fan, Y.; Liu, X. Efficient Inorganic Perovskite Light-Emitting Diodes with Polyethylene Glycol Passivated Ultrathin $CsPbBr_3$ Films. *J. Phys. Chem. Lett.* **2017**, *8*, 4148−4154.
(40) Zhao, Y.; Wei, J.; Li, H.; Yan, Y.; Zhou, W.; Yu, D.; Zhao, Q. A Polymer Scaffold for Self-Healing Perovskite Solar Cells. *Nat. Commun.* **2016**, *7*, 10228.
(41) Meng, Y.; Ahmadi, M.; Wu, X. Y.; Xu, T. F.; Xu, L.; Xiong, Z. H.; Chen, P. High Performance and Stable All-Inorganic Perovskite Light Emitting Diodes by Reducing Luminescence Quenching at PEDOT:PSS/Perovskites Interface. *Org. Electron.* **2019**, *64*, 47−53.
(42) Kim, D. B.; Yu, J. C.; Nam, Y. S.; Kim, D. W.; Jung, E. D.; Lee, S. Y.; Lee, S.; Park, J. H.; Lee, A.-Y.; Lee, B. R.; Di Nuzzo, D.; Friend, R. H.; Song, M. H. Improved Performance of Perovskite Light-Emitting Diodes Using a PEDOT:PSS and $MoO_3$ Composite Layer. *J. Mater. Chem. C* **2016**, *4*, 8161−8165.
(43) Shen, Y.; Li, M.-N.; Li, Y.; Xie, F.-M.; Wu, H.-Y.; Zhang, G.-H.; Chen, L.; Lee, S.-T.; Tang, J.-X. Rational Interface Engineering for Efficient Flexible Perovskite Light-Emitting Diodes. *ACS Nano* **2020**, *14*, 6107−6116.
(44) Yuan, S.; Wang, Z. K.; Xiao, L. X.; Zhang, C. F.; Yang, S. Y.; Chen, B. B.; Ge, H. T.; Tian, Q. S.; Jin, Y.; Liao, L. S. Optimization of Low-Dimensional Components of Quasi-2D Perovskite Films for Deep-Blue Light-Emitting Diodes. *Adv. Mater.* **2019**, *31*, 1904319.
(45) Lian, X.; Wang, X.; Ling, Y.; Lochner, E.; Tan, L.; Zhou, Y.; Ma, B.; Hanson, K.; Gao, H. Light Emitting Diodes Based on Inorganic Composite Halide Perovskites. *Adv. Funct. Mater.* **2019**, *29*, 1807345.
(46) Fan, R.; Song, L.; Hu, Y.; Guo, X.; Liu, X.; Wang, L.; Geng, C.; Xu, S.; Zhang, Y.; Zhang, Z.-H.; Luan, N.; Bi, W. Boosting the Efficiency and Stability of Perovskite Light-Emitting Devices by 3-Amino-1-Propanol Tailored PEDOT:PSS Hole Transport Layer. *ACS Appl. Mater. Interfaces* **2020**, *12*, 43331−43338.
(47) Lin, Z.; Yan, J.; Cai, Q.; Wen, X.; Dong, H.; Mu, C. A Sandwich-Like Electron Transport Layer to Assist Highly Efficient Planar Perovskite Solar Cells. *Nanoscale* **2019**, *11*, 21917−21926.
(48) Jia, Z. W.; Yuan, C. X.; Liu, Y. F.; Wang, X. J.; Sun, P.; Wang, L.; Jiang, H. C.; Jiang, J. Strategies to Approach High Performance in $Cr^{3+}$-Doped Phosphors for High-Power NIR-LED Light Sources. *Light: Sci. Appl.* **2020**, *9*, 86.
(49) Kitazawa, N.; Aono, M.; Watanabe, Y. Synthesis and Luminescence Properties of Lead-Halide Based Organic-Inorganic Layered Perovskite Compounds $(C_nH_{2n+1}NH_3)_2$ $PbI_4$ (N = 4, 5, 7, 8 and 9). *J. Phys. Chem. Solids* **2011**, *72*, 1467−1471.
(50) Guo, Z.; Wu, X.; Zhu, T.; Zhu, X.; Huang, L. Electron-Phonon Scattering in Atomically Thin 2D Perovskites. *ACS Nano* **2016**, *10*, 9992−9998.
(51) Ghosh, S.; Shi, Q.; Pradhan, B.; Kumar, P.; Wang, Z.; Acharya, S.; Pal, S. K.; Pullerits, T.; Karki, K. J. Phonon Coupling with Excitons and Free Carriers in Formamidinium Lead Bromide Perovskite Nanocrystals. *J. Phys. Chem. Lett.* **2018**, *9*, 4245−4250.
(52) Fang, H.-H.; Wang, F.; Adjokatse, S.; Zhao, N.; Even, J.; Antonietta Loi, M. Antonietta Loi, M. Photoexcitation Dynamics in Solution-Processed Formamidinium Lead Iodide Perovskite Thin Films for Solar Cell Applications. *Light: Sci. Appl.* **2016**, *5*, e16056.
(53) Long, H.; Peng, X.; Lu, J.; Lin, K.; Xie, L.; Zhang, B.; Ying, L.; Wei, Z. Exciton-Phonon Interaction in Quasi-Two Dimensional Layered $(PEA)_2(CsPbBr3)_{N-1}PbBr_4$ Perovskite. *Nanoscale* **2019**, *11*, 21867−21871.


https://doi.org/10.1021/acsami.1c02555
*ACS Appl. Mater. Interfaces* 2021, 13, 33199−33208

(54) Xie, C.; You, P.; Liu, Z.; Li, L.; Yan, F. Ultrasensitive Broadband Phototransistors Based on Perovskite/Organic-Semiconductor Vertical Heterojunctions. *Light: Sci. Appl.* **2017**, *6*, e17023.



https://doi.org/10.1021/acsami.1c02555
*ACS Appl. Mater. Interfaces* 2021, 13, 33199−33208